Studying the Stability of a Helical β-Heptapeptide by Molecular Dynamics Simulations

Xavier Daura, Wilfred F. van Gunsteren,* Dario Rigo, Bernhard Jaun* and Dieter Seebach*

Abstract: β-Peptides consisting entirely of homochiral β-amino acids R-CH(NH_2)-CH_2CO_2H form 3_1-helices in solution, as shown previously by NMR analysis of pyridine and methanol solutions. The stability of the helical secondary structure of one such β-peptide (H-β-HVal-β-HAla-β-HLeu-(*S*,*S*)-β-HAla(αMe)-β-HVal-β-HAla-β-HLeu-OH, **1**) has been investigated by molecular dynamics simulations using the GROMOS96 molecular model and force field (962 methanol molecules; $T = 298$, 350, 400 K; with and without NOE distance restraints). The restraints derived from the NMR studies were equally well satisfied by both the restrained and the unrestrained room-temperature molecular dynamics simulations. The 3_1-helical conformation of **1** was shown to be so stable that it was restored spontaneously within 400 ps after unfolding had been induced by a sudden increase of the temperature from 298 to 350 K.

Keywords
helical structures · molecular dynamics simulations · NMR spectroscopy · peptides

Introduction

From numerous single-crystal X-ray structures of oligolides from (*R*)-3-hydroxybutanoic acid (**A** in Scheme 1), we had concluded that there should be a favourable helical backbone conformation of linear oligo- and polyesters built from 3-hydroxyalkanoate (**B** in Scheme 1). Modelling studies showed that, with building blocks of (*R*) configuration, a (*P*) helicity and a pitch of approximately 6 Å in a 3_1-helix should result[1] (see Scheme 1). By means of fibre X-ray scattering investigations, the polyesters from (*R*)-3-hydroxybutyrate (PHB) and -valerate (PHV) have been shown to form 2_1-helices (ca. 6 Å pitch, (*M*) chirality), but the modelled 3_1-helix has not been observed experimentally.[2] Additionally, there is no evidence for secondary-structure formation in solutions of the linear and cyclic oligomers of these hydroxy acids, at least not on the NMR timescale.[1, 2] Upon inspection of the modelled PHB 3_1-helix we noticed, however, that carbonyl and backbone oxygens are in rather close proximity (separated by ca. 2.9 Å), and therefore we thought that replacement of the backbone oxygen by an NH should lead to hydrogen bonding and thus stabilisation of the helix. To our surprise, a literature search revealed that no systematic study had been published on oligomers of 3-aminocarboxylic acids. We therefore embarked in a general investigation of β-amino acids and β-peptides, to find out that oligomers containing as few as six β-amino acid residues form stable helices, identified by CD and NMR spectroscopy,[3–5] and that it is not necessary to reduce the conformational flexibility of the backbone of such β-peptides[6] to observe the helix in methanol solution. Detailed NMR analysis in this solvent of a β-hexapeptide and the β-heptapeptide **1** (see Scheme 1), synthesised from β-amino acids obtained by Arndt–Eistert homologation of the (*S*)- (or L-) α-amino acids, confirmed the helical structure of such β-peptides[4] (a left-handed (or *M*) 3_1-helix of 5 Å pitch), previously discovered in pyridine solution.[3] The remarkable stability of this helix follows also from the slow H/D exchange of the central NH hydrogens in CH_3OD. It is specially revealing that, despite of the additional α-methylene group in the β-amino acids, the β-peptides studied are more structured than the analogous α-peptides.

We now describe detailed molecular dynamics simulation studies of the β-heptapeptide **1** in methanol solution, with and without NOE distance restraints, at three different temperatures, using the GROMOS96 force field and molecular model.[7] Owing to the nature of the molecular system under study, this is also a good test case for this force field.

[*] W. F. van Gunsteren, X. Daura
Laboratorium für Physikalische Chemie, Eidgenössische Technische Hochschule
ETH-Zentrum, CH-8092 Zürich (Switzerland)
Fax: Int. code +(1)632-1039
e-mail: wfvgn@igc.phys.chem.ethz.ch
B. Jaun, D. Seebach, D. Rigo
Laboratorium für Organische Chemie, Eidgenössische Technische Hochschule
ETH-Zentrum, CH-8092 Zürich (Switzerland)
Fax: Int. code +(1)632-1144
e-mail: jaun@org.chem.ethz.ch or seebach@org.chem.ethz.ch

Results and Discussion

Four molecular dynamics (MD) simulations were carried out, with the aim of studying the stability of the (left-handed) helical structure that the NMR studies[4] determined for this β-heptapeptide in methanol. The first of the MD simulations

0947-6539/97/0309-1410 $ 17.50+.50/0

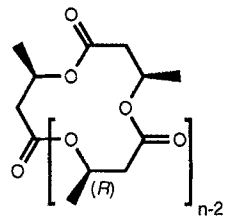

A (oligolide from (*R*)-3-hydroxybutanoic acid)

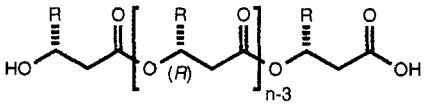

B (linear poly((*R*)-3-hydroxyalkanoate)

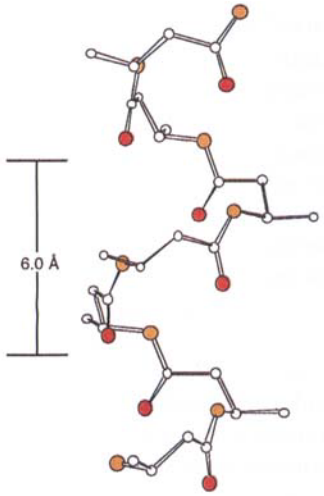

(*P*)-3_1-helix of **B**

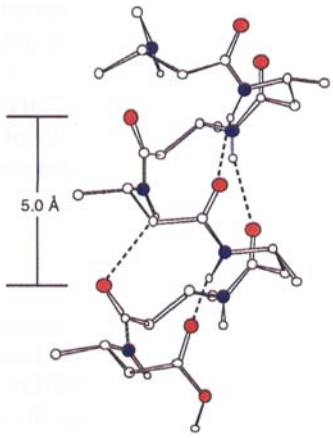

(*M*)-3_1-helix of a β-peptide such as **1**

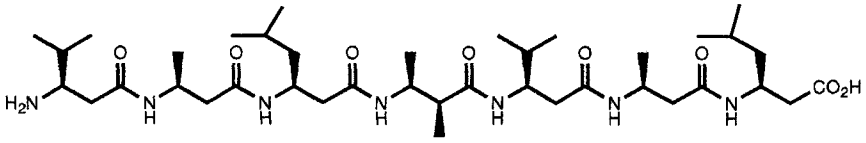

H-β-HVal-β-HAla-β-HLeu-(*S*,*S*)-β-HAla(αMe)-β-HVal-β-HAla-β-HLeu-OH (**1**)

Scheme 1. Structural comparison of oligomers from β-hydroxy- and β-amino acids. **A**: cyclic oligomer (oligolide); **B**: linear oligomer of (*R*)-3-hydroxyalkanoic acids, PHB (R = CH_3), PHV (R = C_2H_5); (*P*) and (*M*) 3_1-helices of the polyester (modelled [1,2]) and of the corresponding polyamide (from NMR measurements [3–6]); **1**: β-heptapeptide used for the molecular dynamics simulations described here (H in front of amino acid symbol represents the prefix "homo").

(MDDR) served as a reference simulation. It was set up at 298 K (room temperature), with a time-averaged restraining procedure to force the peptide to satisfy (on average) the NOE distances derived from experiment. The other three were standard (unrestrained) MD simulations at different temperatures, namely, 298 K (MDT1), 350 K (MDT2) and 400 K (MDT3). We should emphasise at this point that the GROMOS96 force field, like most others, has been parametrised for room-temperature simulation and, therefore, the use of high temperatures in the MDT2 and MDT3 simulations should be viewed as a way to introduce energy into the system, increasing the motion of the atoms, and to induce destabilisation of the helix, rather than as a picture of the physical behaviour of the real system at the high temperatures.

The analysis of the resulting trajectories shows that the 3_1-helix is indeed very stable in the GROMOS96 force field, suggesting that this may also be the case for the peptide in vitro. The average dynamic and structural properties of the peptide in simulation MDT1 are very similar to those in simulation MDDR even though there were no restraints driving the peptide towards a target structure. In simulation MDT2, the initial temperature shock temporarily destroys the helical structure of the peptide, but this is fully recovered after the first 500 ps period. Permanent destabilisation of the helix through temperature increase is only achieved by keeping the system at 400 K for longer than 800 ps in simulation MDT3.

In Figure 1 we have plotted the root mean square (RMS) positional deviation of the peptide backbone atoms from the initial model structure as a function of the simulation time, calculated for each of the four trajectories. This gives an impression of the overall structural differences between the initial model structure (defined in the section Computational Methods) and each of the structures extracted sequentially from the trajectory. In simulations MDDR and MDT1 the structure of the peptide always remains close to the initial model one (RMS deviation around 0.1 nm). Nevertheless, while the value of the RMS deviation is quite stable in simulation MDDR, it shows a slightly more fluctuating behaviour in simulation MDT1. Periods of time in which the tails of the peptide move around the region of conformational space defined by the initial model structure alternate with periods of time in which they move away to visit distinctly different neighbouring regions (this can be seen in Figure 3). These long-range oscillations of the peptide tails are more restricted in simulation MDDR due to the presence of distance restraints. In simulation MDT2 there is an initial period in which the RMS deviation values are large, due to partial unfolding induced by the sudden change in temperature. Nevertheless, and quite surprisingly considering the degree of unfolding already reached, after about 300 ps the peptide starts to recover its initial conformation. Beyond the first 500 ps, the RMS deviation from the initial model structure shows a pattern similar to that of the MDT1 simulation, although with larger fluctuations due to the higher temperature, and always returning to RMS values of around 0.06 nm. In simulation MDT3 the initial temperature shock does not destroy the helical conformation. The peptide stays more or less close to the initial structure during grossly the first 1000 ps, with RMS deviation values between 0.1 and 0.3 nm. This does not necessarily mean that the essential features of the helix are always present. After that period of time the peptide loses completely its initial fold and never recovers a structure with low RMS deviation values from the initial model structure. On the basis of Figure 1, the following periods of time were considered

  0947-6539/97/0309-1411 $ 17.50+.50/0

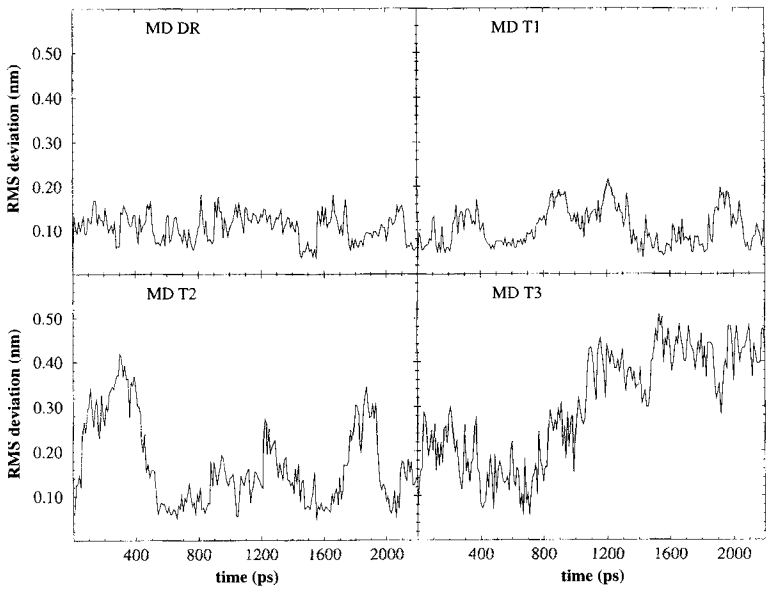

Figure 1. Root mean square (RMS) positional deviation of the backbone atoms from their initial (model structure) positions as a function of the simulation time. Before the calculation of the RMS deviation, the conformations extracted from the trajectories were least-squares fitted to the initial model structure by using the coordinates of the backbone atoms of residues 2 to 6.

whenever the analysis required averaging: between 100 and 2200 ps in simulations MDDR and MDT1, and between 500 and 2200 ps in simulation MDT2. We divided simulation MDT3 somewhat arbitrarily into two stages, one between 0 and 1000 ps (MDT3-H) and one between 1000 and 2200 ps (MDT3-C).

The radius of gyration of the peptide as a function of the simulation time (Figure 2) gives different structural information. The radius of gyration is a function of the RMS distance of the atoms from their common centre of gravity, and is therefore related to the size and shape of the molecule. In simulations MDDR and MDT1 the radius of gyration oscillates near its initial value during the whole simulation. In simulation MDT2, an initial elongation of the structure accompanies the increase of the RMS deviation from the initial model structure observed in Figure 1. The oscillations observed in the RMS deviation values correlate with those in the radius of gyration. In simulation MDT3, after a first 800 ps period in which the radius of gyration presents a profile similar to that of simulation MDT2, the 3_1-helix unfolds in two stages, one (from about 900 to 1500 ps) in which it reaches an almost completely extended shape, with radius of gyration values up to 0.75 nm, and a second (from about 1600 to 2200 ps) in which the radius of gyration decreases again, even though the RMS deviation from the initial model structure is still slightly increasing, indicating that the peptide has adopted a non-helical (in this case random coil like) fold.

To obtain a visual picture of the behaviour of the system in the simulations (information already implicit in Figures 1 and 2), we show in Figure 3 a representation of the backbone of the initial model structure as well as a superposition of structures extracted at the times 300, 600, 900, 1200, 1500, 1800 and 2100 ps from the different trajectories. As indicated by the time course of the RMS deviation and the radius of gyration, in simulations MDDR and MDT1 the core of the peptide (residues 2 to 6) keeps the same basic structure along the whole trajectory, and only the tails present larger-scale movements, especially in simulation MDT1. The conformations extracted from simulation MDT2 present more dispersion in their superposition due to the increase in the fluctuations induced by the higher temperature, but they still do individually represent a helical structure (with the exception of the conformation extracted at time 300 ps). There is no reasonable least-squares fitting of the atom positions possible for the conformations extracted from simulation MDT3, with structures that are still partially a left-handed helix (at 300 and 600 ps), others that are almost totally extended (at 900, 1200 and 1500 ps) and a third group that adopts a non-native fold (at 1800 and 2100 ps).

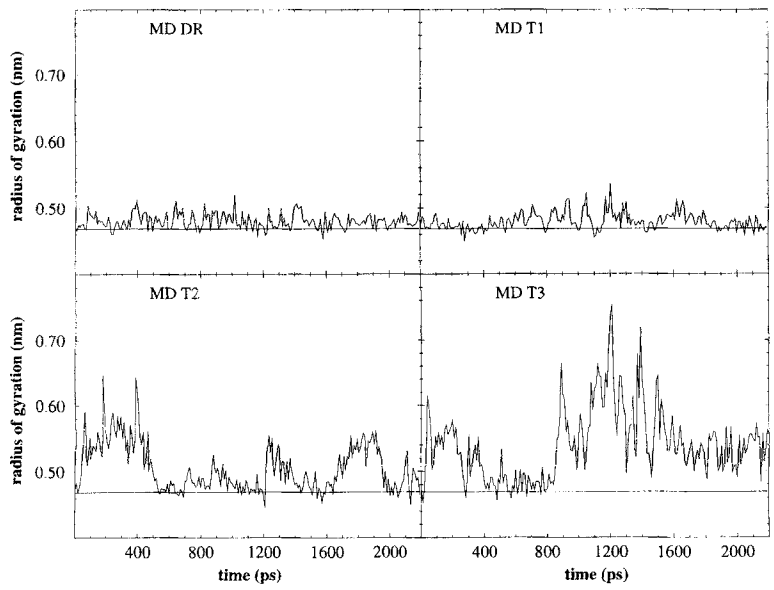

Figure 2. Radius of gyration of the peptide as a function of the simulation time. The horizontal line corresponds to the radius of gyration of the initial model structure.

The RMS positional fluctuations of the backbone atoms are shown in Figure 4 for each of the simulations. As one could already guess from the superpositions of structures in Figure 3, the profile of the RMS fluctuations is very similar in simulations MDDR and MDT1: relatively small fluctuations in the core region (residues 2 to 6) and a bit larger fluctuations in the two tails, especially in the C-terminal one. In simulation MDT2 the average fluctuations of the backbone atoms in the core region are almost twice as high as in the simulations at room temperature. The two tails are also more mobile, the N-terminal one apparently being the most affected by the increase in temperature. In the MDT3-H simulation the RMS positional fluctuations of the backbone atoms are only a bit larger than in simulation MDT2, with an even more mobile N-terminus. In the MDT3-C simulation the RMS fluctuations are about four times higher than in simulations MDDR and MDT1. The actual profile of the RMS fluctuations is in this case not significant, since the distribution of the RMS fluctuations along the backbone is, in MDT3-C, highly dependent on the way the superposition of like

0947-6539/97/0309-1412 $ 17.50+.50/0 Chem. Eur. J. 1997, 3, No. 9

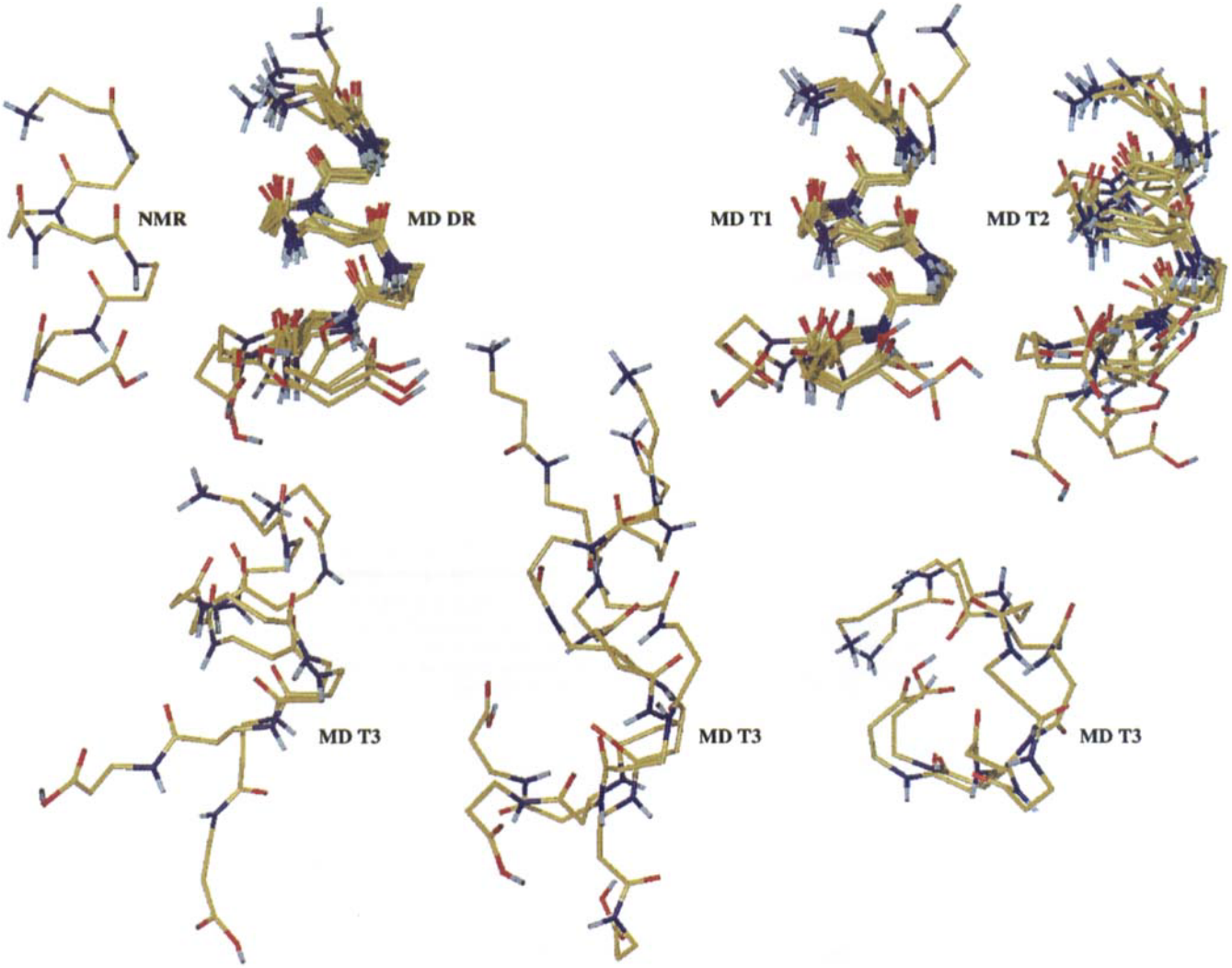

Figure 3. Superposition of conformations extracted from the simulations. NMR refers to the initial model structure. Seven conformations were extracted from each of the trajectories, at times 300, 600, 900, 1200, 1500, 1800, and 2100 ps, and superimposed by least-squares fitting of the backbone atoms of residues 2 to 6. The conformations from simulation MDT3 have been classified in three groups according to their approximate folds. The first group (from left to right) contains the conformations extracted at times 300 and 600 ps, the second one contains the conformations extracted at times 900, 1200 and 1500 ps, and the third one contains the conformations extracted at times 1800 and 2100 ps.

atoms is performed, owing to the very different shapes that the peptide adopts in this stage of the simulation (see Figure 3).

To evaluate the degree of agreement between the conformations sampled in the two simulations at room temperature and the NOE distances derived from the NMR experiments, we have plotted in Figure 5 the average effective violations of the NOE distances for the initial model structure and for simulations MDDR and MDT1. Even though the experimental NOEs were obtained at a lower temperature (298 K), we have also plotted the average effective violations for simulations MDT2 and MDT3 (divided in plots MDT3-H and MDT3-C), since this will show how the helical information is distributed in the NOEs and how the peptide loses this information in the last 1200 ps of simulation MDT3. The negative violations correspond to distances that are smaller in the computationally obtained conformations (including the initial model structure) than the ones predicted by the NMR data, and the positive violations correspond to distances that are bigger in the computationally obtained conformations. The NMR (initial model) structure has six violations that are clearly over 0.05 nm (in absolute value), approximately the average estimated error in the experimental NOE distances, which correspond to the sequence numbers 9, 22, 24, 28, 29 and 31 (see Table 1). One may consider the first five of these six violations as being the result of using conservative upper bounds when translating the strong, medium and weak NOEs into upper-distance limits. The cross-peaks corresponding to NOEs 9 and 29 had a COSY-type (antiphase) component, which made the translation difficult. On the other hand, the NOEs 9, 22 and 28 involve CH_3 groups, in which case the distances in the model structure must refer to a pseudo atom. This may also be a possible source of error, even though there is a correction term for the distances in order to account for it. The NOE 31, between NH(5) and NH(6), gives a distance that, as we will see, could not be satisfied by either the model structure or by the unrestrained simulation. The positive violations observed for the NMR structure have been flattened by the use of distance restraints in simulation MDDR. Those negative violations which in the initial model structure were bigger than 0.05 nm in absolute value, are also present here (sequence numbers 9, 22, 24, 28, 29). We should emphasise that we have used

  0947-6539/97/0309-1413 $ 17.50+.50/0

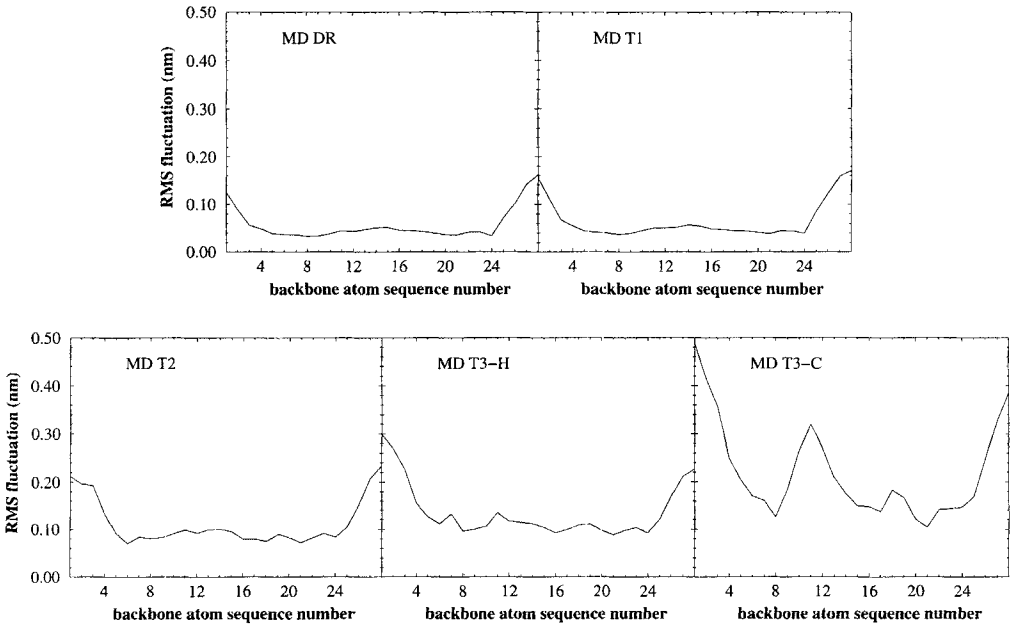

Figure 4. Root mean square (RMS) positional fluctuations of the backbone atoms. Before the calculation of the RMS fluctuations, the conformations extracted from the trajectories were least-squares fitted to the initial model structure using the coordinates of the backbone atoms of residues 2 to 6. The RMS differences between the average structure from each of the simulations and the initial model structure are, for the backbone atoms and for all atoms, respectively, the following: 0.86/1.66 nm in MDDR, 0.83/1.56 nm in MDT1, 0.81/1.51 nm in MDT2, 1.16/1.96 nm in MDT3-H and 3.30/4.02 nm in MDT3-C.

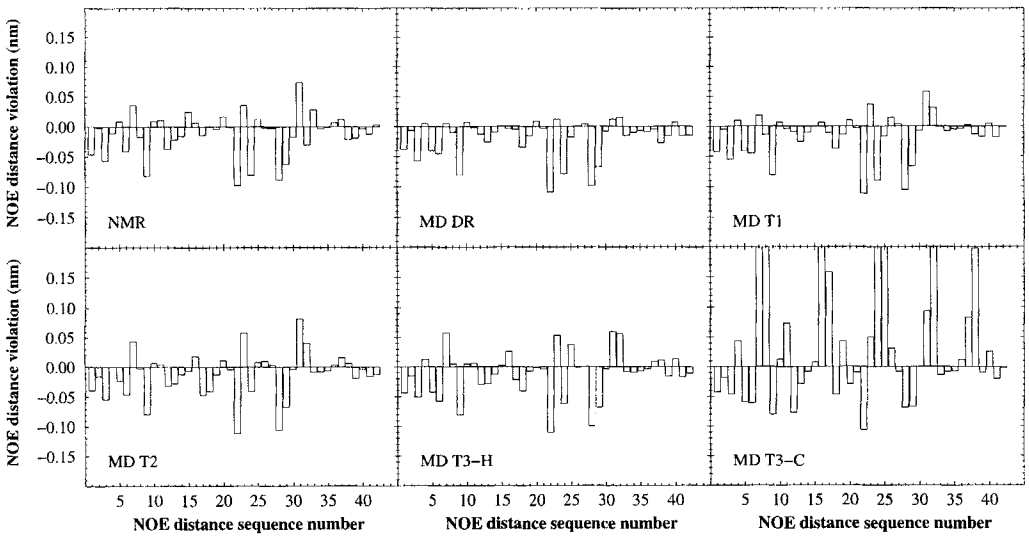

Figure 5. Effective violations of experimental NOE distances. Difference between 42 experimental NOE distances (obtained for the system at room temperature) and the corresponding average distances calculated from the simulations. The sum of the positive violations in the initial model structure and in each of the simulations is the following: 0.29 nm in NMR, 0.08 nm in MDDR, 0.20 nm in MDT1, 0.31 nm in MDT2, 0.35 nm in MDT3-H and 3.00 nm in MDT3-C.

an attractive interaction term for the restraining, so that negative violations (if in this case they can be called violations at all) are permitted. In the MDT1 simulation the pattern of negative violations is almost identical to that observed in the MDDR simulation. The distance with sequence number 31 is here slightly over 0.05 nm larger than the NOE-derived distance, as already mentioned. In the MDT2 simulation the average effective violations are similar in range to the ones shown for the MDT1 simulation, reinforcing the impression that in this simulation the average structural properties of the peptide were only slightly affected by the increase in the temperature (except for the initial 300 ps period), even though the atomic fluctuations were much larger than those at 298 K. No large positive violations are found in simulation MDT3-H either, and the pattern of negative violations also remains close to that of the initial model structure. In the MDT3-C simulation there are a number of large positive violations that correspond to distances that increase as the helical structure is lost, that is, long-range (in chain sequence) NOEs. The NOE distances with sequence numbers 7 and 8 (see Table 1), with average violations of 0.34 and 0.45 nm, respectively, correspond to weak NOEs in the helical structure between NH(2) (N hydrogen of residue 2) and H–C_β(4) (C_β

0947-6539/97/0309-1414 $ 17.50+.50/0 Chem. Eur. J. 1997, 3, No. 9

Table 1. NOE distances.

s [a]	H atoms [b]		d [c]	s [a]	H atoms [b]		d [c]
1	NH(1)	$H-C_\beta(1)$	0.28	22	NH(4)	$H-C_\gamma(4)$	0.30
2	$H-C_\beta(1)$	$H_{ax}-C_\alpha(1)$	0.29	23	NH(4)	$H-C_\beta(6)$	0.32
3	$H-C_\beta(1)$	$H_{eq}-C_\alpha(1)$	0.30	24	NH(4)	$H-C_\beta(7)$	0.37
4	NH(2)	$H_{ax}-C_\alpha(1)$	0.24	25	$H-C_\beta(4)$	$H_{ax}-C_\alpha(1)$	0.26
5	NH(2)	$H_{eq}-C_\alpha(1)$	0.29	26	NH(5)	NH(4)	0.37
6	NH(2)	$H-C_\beta(2)$	0.33	27	NH(5)	$H_{ax}-C_\alpha(4)$	0.22
7	NH(2)	$H-C_\beta(4)$	0.35	28	NH(5)	$Me-C_\alpha(4)$	0.35
8	NH(2)	$H-C_\beta(5)$	0.33	29	NH(5)	$H-C_\beta(5)$	0.35
9	$H-C_\beta(2)$	$H-C_\gamma(2)$	0.22	30	NH(5)	$H_{ax}-C_\alpha(5)$	0.25
10	$H-C_\beta(2)$	$H_{eq}-C_\alpha(2)$	0.23	31	NH(5)	NH(6)	0.35
11	NH(3)	$H_{ax}-C_\alpha(2)$	0.22	32	$H-C_\beta(5)$	$H_{ax}-C_\alpha(2)$	0.23
12	NH(3)	$H_{eq}-C_\alpha(2)$	0.31	33	$H-C_\beta(5)$	$H-C_\gamma(5)$	0.26
13	NH(3)	$H-C_\beta(3)$	0.31	34	$H-C_\beta(5)$	$H_{eq}-C_\alpha(5)$	0.25
14	NH(3)	$H_{ax}-C_\alpha(3)$	0.26	35	NH(6)	$H-C_\beta(6)$	0.29
15	NH(3)	NH(4)	0.38	36	NH(6)	$H_{ax}-C_\alpha(6)$	0.25
16	NH(3)	$H-C_\beta(5)$	0.34	37	NH(6)	$H_{ax}-C_\alpha(5)$	0.22
17	NH(3)	$H-C_\beta(6)$	0.32	38	$H-C_\beta(6)$	$H_{ax}-C_\alpha(3)$	0.25
18	$H-C_\beta(3)$	$H-C_\delta(3)$	0.30	39	$H-C_\beta(6)$	$H_{eq}-C_\alpha(6)$	0.26
19	NH(4)	$H_{ax}-C_\alpha(3)$	0.23	40	NH(7)	$H_{ax}-C_\alpha(6)$	0.24
20	NH(4)	$H_{eq}-C_\alpha(3)$	0.28	41	NH(7)	$H-C_\beta(7)$	0.30
21	NH(4)	$H-C_\beta(4)$	0.29	42	NH(7)	$H_{ax}-C_\alpha(7)$	0.27

[a] Sequence number of NOE distance. [b] The residue sequence numbers of the atoms are indicated in parentheses. [c] NOE distance in nm.

hydrogen of residue 4) and between the same NH(2) and $H-C_\beta(5)$. The sequence numbers 16 and 17, with average violations of 0.29 and 0.16 nm, respectively, correspond again to weak NOEs in the helical structure between NH(3) and $H-C_\beta(5)$ and between NH(3) and $H-C_\beta(6)$. The sequence numbers 24 and 25, with average violations of 0.28 and 0.54 nm, respectively, correspond to the weak NOE between NH(4) and $H-C_\beta(7)$ and to the strong NOE between $H-C_\beta(4)$ and $H_{ax}-C_\alpha(1)$ (C_α axial hydrogen of residue 1). Interestingly, the weak NOE between NH(4) and $H-C_\beta(6)$ (sequence number 23) presents a low violation, even though the NOE distance between NH(3) and $H-C_\beta(6)$, which should be of the same size in the helical structure, is clearly violated. This can only be explained in terms of a different type of fold. Finally, the NOE distance sequence numbers 32 and 38, with average violations of 0.31 and 0.20 nm, respectively, correspond to strong NOEs in the helical structure between $H-C_\beta(5)$ and $H_{ax}-C_\alpha(2)$, and between $H-C_\beta(6)$ and $H_{ax}-C_\alpha(3)$. The violations of the NOE distances with sequence numbers 11, 19 and 37, between an NH and the $H_{ax}-C_\alpha$ in the preceding residue, and 31, between NH(5) and NH(6), also become sizeable at this stage of the simulation. Of the central NH to $H_{ax}-C_\alpha$ distances, only the one between NH(5) and $H_{ax}-C_\alpha(4)$ (sequence number 27) is on average not violated, possibly indicating that there is still part of the central turn present in the new folds.

We have also compared 21 experimental ^3J coupling constants derived from experiment with their average values in the simulations (Figure 6), calculated with the Karplus equation[8] [Eq. (1) in Computational Methods]. The upper-left plot compares the experimental ^3J coupling constants with the ones calculated for the initial model structure. The first range of experimental ^3J coupling constant values (between 2 and 5 Hz) contains the ^3J coupling constants for the pairs $H-C_\beta/H_{eq}-C_\alpha$ (C_β hydrogen, C_α equatorial hydrogen), which are generally a bit too small in the initial model structure (see Table 2). This is due to dihedral angles which, according to the Karplus curve, are about 10° larger than expected from the experimental ^3J coupling constants, namely, between 60 and 70° instead of between 50 and 60°. The second range of experimental ^3J coupling constant values (between 4 and 8 Hz) contains values for the pairs $H-C_\beta/H-C_\gamma$ from residues 1 βVal and 5 βVal, which are very high in the initial model structure. This is due to the arbitrary choice of rotamers for the side chains in this structure, with a dihedral angle of about 180° between the two hydrogens. The third range of experimental ^3J coupling constant values (be-

Table 2. ^3J coupling constants.

s [a]	H atoms [b]		^3J [c]	s [a]	H atoms [b]		^3J [c]
1	$H-C_\beta(1)$	$H_{eq}-C_\alpha(1)$	2.8	12	NH(5)	$H-C_\beta(5)$	9.6
2	$H-C_\beta(2)$	$H_{eq}-C_\alpha(2)$	4.5	13	NH(6)	$H-C_\beta(6)$	8.7
3	$H-C_\beta(3)$	$H_{eq}-C_\alpha(3)$	4.5	14	NH(7)	$H-C_\beta(7)$	9.5
4	$H-C_\beta(5)$	$H_{eq}-C_\alpha(5)$	3.9	15	$H-C_\beta(1)$	$H_{ax}-C_\alpha(1)$	11.5
5	$H-C_\beta(6)$	$H_{eq}-C_\alpha(6)$	3.8	16	$H-C_\beta(2)$	$H_{ax}-C_\alpha(2)$	12.0
6	$H-C_\beta(7)$	$H_{eq}-C_\alpha(7)$	4.5	17	$H-C_\beta(3)$	$H_{ax}-C_\alpha(3)$	12.3
7	$H-C_\beta(1)$	$H-C_\gamma(1)$	4.7	18	$H-C_\beta(4)$	$H_{ax}-C_\alpha(4)$	10.8
8	$H-C_\beta(5)$	$H-C_\gamma(5)$	7.0	19	$H-C_\beta(5)$	$H_{ax}-C_\alpha(5)$	12.3
9	NH(2)	$H-C_\beta(2)$	9.2	20	$H-C_\beta(6)$	$H_{ax}-C_\alpha(6)$	11.6
10	NH(3)	$H-C_\beta(3)$	9.6	21	$H-C_\beta(7)$	$H_{ax}-C_\alpha(7)$	10.0
11	NH(4)	$H-C_\beta(4)$	9.3				

[a] Sequence number of ^3J coupling constant. [b] The residue sequence numbers of the atoms are indicated in parentheses. [c] ^3J coupling constant in Hz.

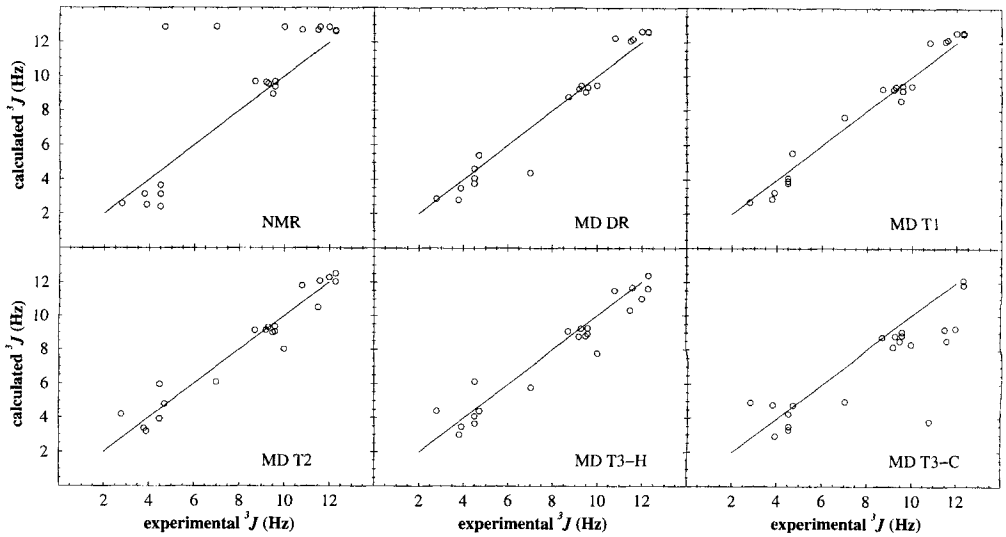

Figure 6. Calculated versus experimental ^3J coupling constants. Comparison of 21 experimental ^3J coupling constants (obtained for the system at room temperature) with the corresponding average ^3J coupling constants calculated from the simulations. The straight line stands for identity. The sum of the (absolute) differences between the experimental and calculated ^3J coupling constants are, for the initial model structure and for each of the simulations, the following: 32.1 Hz for NMR, 11.6 Hz for MD DR, 11.1 Hz for MD T1, 13.2 Hz for MD T2, 15.8 Hz for MD T3-H and 29.9 Hz for MD T3-C.

  0947-6539/97/0309-1415 $ 17.50+.50/0

tween 8 and 10 Hz) contains values for the pairs NH/H–C_β, for which there is general good agreement between model structure and experiment, with dihedral angles around 180°. The last range of experimental ^3J coupling constant values (between 10 and 13 Hz) contains values for the pairs H–C_β/H_{ax}–C_α, which are generally a bit too high in the initial model structure, as expected, since they are coupled with the same dihedral angle as the H–C_β/H_{eq}–C_α pair. In this case, the dihedral angle between the two hydrogens is about 180 and 190° instead of 170 and 180°, predicted from the Karplus curve. In plots MDDR and MDT1 the points mostly lie very close to the straight line, that is, there is close agreement between the experimental and simulated ^3J coupling constants. This is especially remarkable for simulation MDT1, where, in the absence of restraints, the force field generates the proper dihedral angle distributions, even for the side chains. In plots MDT2 and MDT3-H there is also quite good agreement between the experimental and the average calculated ^3J coupling constants, although with an expected higher dispersion. In plot MDT3-C, the average calculated ^3J coupling constants for the hydrogen pairs NH/H–C_β and H–C_β/H_{ax}–C_α are smaller, as the dihedral angles deviate, with unfolding of the peptide, from the value that corresponds to a maximum ^3J value in the Karplus curve, that is, about 180° in both cases.

The picture of the peptide conformations and dynamics is completed with the calculation of intramolecular hydrogen bonding propensities. In Table 3 we show their occurrences in the simulations. As a complement, Table 4 shows detailed hydrogen bonding data from simulation MDT1. The most important hydrogen bonds supporting the helical structure are the three central ones, NH(2)–O(4) (N hydrogen of residue 2 and C oxygen of residue 4), NH(3)–O(5) and NH(4)–O(6), which are present in the initial model structure and with high occurrences and long (in relative terms) lifetimes in simulations MDDR and MDT1. In particular, the NH(3)–O(5) and NH(4)–O(6) hydrogen bonds appear to be especially stable in these two simulations (see also Table 4). The occurrences of these three hydrogen bonds are lower in simulation MDT2 and in the first period of simulation MDT3 (MDT3-H); the central NH(3)–O(5) hydrogen bond is the most resistant to high temperatures. The three of them, however, disappear completely in the second part of simulation MDT3 (MDT3-C). The two extreme (in the helix) hydrogen bonds, NH(1)–O(3) and NH(5)–O(7), are observed less frequently in the simulations, owing to the mobility of the peptide tails. The polar atoms that are most exposed and at the same time have more stable hydrogen bonds with the solvent are the O(2), NH(6) and NH(7) (see Table 4). The O(1) and the terminal NH and O atoms are also exposed to the solvent, but the high mobility of the tails prevents them from establishing many stable hydrogen bonds. Another interesting feature common to simulations MDDR and MDT1 is that the N(1) (terminal nitrogen) atom spends more time hydrogen bonded to solvent than to peptide oxygens, while the reverse is true for the O1(7) (unprotonated terminal oxygen) and O2(7) (protonated terminal oxygen) atoms.

Table 3. Intramolecular hydrogen bonds.

Donor [a]	Acceptor [b]	NMR [c]	MDDR [c]	MDT1 [c]	MDT2 [c]	MDT3-H [c]	MDT3-C [c]
NH(1)	O(2)	+	..	..	–	–	–
NH(1)	O(3)	+	23.7	22.0	24.6	17.6	–
NH(2)	O(4)	+	91.1	85.0	68.1	54.5	–
NH(3)	O(5)	+	95.1	93.0	84.6	71.7	–
NH(4)	O(5)	–	–	..	..	..	26.8
NH(4)	O(6)	+	96.0	92.0	60.7	62.6	–
NH(5)	O1(7)	–	19.9	15.8	10.2	–	..
NH(5)	O2(7)	+	..	6.0	15.3	–	..
NH(7)	O(5)	–	–	–	..	–	22.8

[a] The residue sequence numbers of the atoms are indicated in parentheses. [b] Presence (+) or absence (–) of a hydrogen bond. [c] Occurrence (%) of a hydrogen bond: a hydrogen bond is considered to exist when the donor–hydrogen–acceptor angle is larger than 135° and the hydrogen–acceptor distance is smaller than 0.25 nm; only those hydrogen bonds occurring in more than 5% of the analysed conformations have been considered.

Table 4. Hydrogen bond occurrences in simulation MDT1 and their relative lifetimes.

	Hydrogen bonds to peptide atoms				Hydrogen bonds to solvent atoms				Total	
Atom [a]	p [b]	n [c]	Max. [d]	$<t>$ [e]	p [b]	n [c]	Max. [d]	$<t>$ [e]	p [b]	$<t>$ [e]
NH1(1)	278	182	4.5	1.0	3002	997	23.5	1.5	3273	1.5
NH2(1)	357	217	11.5	1.0	2910	1019	12.5	1.5	3254	1.5
NH3(1)	359	216	10.0	1.0	2978	929	20.5	1.5	3327	1.5
NH(2)	3572	461	28.5	4.0	102	88	1.5	0.5	3673	3.5
NH(3)	3921	273	72.0	7.0	33	31	1.0	0.5	3953	6.5
NH(4)	3906	225	66.5	8.5	50	15	6.5	1.5	3956	8.5
NH(5)	919	339	8.0	1.5	2534	358	40.5	3.5	3442	2.5
NH(6)	16	11	2.0	0.5	3663	408	40.5	4.5	3679	4.5
NH(7)	0	0	0.0	0.0	3646	474	38.5	4.0	3646	4.0
O(1)	37	34	1.5	0.5	837	304	11.5	1.5	869	1.5
O(2)	31	25	2.0	0.5	3311	526	24.5	3.5	3341	3.0
O(3)	929	559	11.5	1.0	594	136	13.0	2.0	1520	1.0
O(4)	3579	476	28.5	4.0	3	2	1.0	0.5	3579	4.0
O(5)	3906	263	72.0	7.5	122	41	5.5	1.5	3919	6.5
O(6)	3868	196	66.5	10.0	159	37	11.5	2.0	3947	8.5
O1(7)	699	269	8.0	1.5	200	109	4.0	1.0	898	1.0
O2(7)	271	102	5.5	1.5	199	70	7.0	1.5	470	1.5

[a] The residue sequence numbers of the atoms are indicated in parentheses. [b] Number of conformations (out of 4200 conformations extracted from the simulation period of 100–2200 ps) in which the indicated atom is hydrogen bonded (as donor if it is a nitrogen or as acceptor if it is an oxygen) to another peptide atom (column 2), to a solvent atom (column 6) and to any of the latter two (column 10). [c] Number of times the indicated atom establishes a new hydrogen bond during the time period considered; a given hydrogen bond is considered to be broken if it disappears for longer than 0.5 ps (the resolution of the analysis) or if the donor or the acceptor atoms are substituted by a different one. [d] Maximum lifetime (in ps) of the hydrogen bonds established by the indicated atom with other peptide atoms (column 4) and with solvent atoms (column 8). [e] Average lifetime (in ps).

0947-6539/97/0309-1416 $ 17.50+.50/0 *Chem. Eur. J.* **1997**, *3*, No. 9

Conclusions

We have performed MD simulations on a β-heptapeptide in methanol at three different temperatures, namely, 298, 350 and 400 K. This peptide was found by NMR structure-determination studies to adopt a 3_1-helix in this solvent. The molecular model, for both solute and solvent, and the force field used in the simulations were those of GROMOS96. The simulations show that, in the context of this force field and molecular model, the 3_1-helix is not only stable at 298 K, but also remarkably resistent to unfolding with increasing temperature. Strikingly, there is no qualitative (and hardly any average-quantitative) difference between the two simulations at room temperature, even though 42 NOE distance restraints derived from the NMR experiments were applied in the first and none in the second. Both were equally consistent with the experimental observations. Furthermore, after a sudden increase of the temperature to 350 K, which induced the unfolding of the 3_1-helix, the peptide spontaneously and rapidly (in about 200 ps) recovered its helical conformation; this result indicates that the latter conformation is most probably strongly favoured for this peptide in methanol when the above-mentioned force field is used. Detailed analysis of the sequence of structures obtained from the high-temperature trajectories suggests that spontaneous refolding is possible as long as the central turn is at least partially present, even if the hydrogen bond between the NH(3) and the O(5) atoms, which closes this turn, is not formally present. Permanent destabilisation of the helix was only achieved after the temperature had been raised to 400 K and maintained at this value for longer than 800 ps.

Computational Methods

All simulations and analyses reported here were performed within the framework of the GROMOS96 package of programs.[7] The GROMOS96 molecular model and force field[7] were used throughout for the evaluation of the forces.

Molecular model and simulation set-up: As starting point for our calculations we used a model structure of the backbone of the β-heptapeptide built by Seebach et al.[4] based on NMR structure-determination studies. The rotamers of the side chains were arbitrarily chosen. The end groups were chosen to be protonated (-NH_3^+ and -COOH), the most probable state according to the experimental data. This model structure was placed in the centre of a rectangular box, the size of which was chosen such that the minimum distance from any peptide atom to the wall was 1.4 nm. The solvent was then introduced into the box by using as a building block a cubic configuration of 216 equilibrated methanol molecules. All methanol molecules with the oxygen atom lying within 0.3 nm of a non-hydrogen peptide atom were then removed. In this way, a total of 962 methanol molecules were introduced into the system. Rectangular periodic boundary conditions were applied.

In order to relax the first shells of methanol molecules around the peptide, we performed a steepest-descent energy minimisation of the system, keeping the peptide atoms positionally restrained using a harmonic interaction with a force constant of 25 kJ mol^{-1} nm^{-2}. After that, we performed a second steepest-descent energy minimisation of the whole system without restraints to eliminate any residual strain.

Two MD simulations of the β-heptapeptide in methanol were then set up, one at 298 K with time-averaged NOE distance restraints (MD DR) and one at 298 K (MDT1). To start up the MD simulations, the initial velocities of the atoms were taken from a Maxwellian distribution at 298 K. The peptide and the solvent were, independently, weakly coupled to a temperature of 298 K with a relaxation time of 0.1 ps.[9] Parallel to that, the entire system was weakly coupled to a pressure of 1 atm with a relaxation time of 0.5 ps.[9] Bond lengths were constrained to equilibrium values using the SHAKE algorithm,[10] with a geometric tolerance of 10^{-4}. Not having to account for bond vibrations, the time step for the leap-frog integration scheme was set to 0.002 ps. The non-bonded interactions were evaluated by means of a twin-range method: The short-range van der Waals and electrostatic interactions were evaluated at every time step, by using a charge-group pair list that was generated with a short-range cut-off radius of 0.8 nm. Longer-range van der Waals and electrostatic interactions (between charge groups at a distance longer than the short-range cut-off and shorter than a long-range cut-off of 1.4 nm) were evaluated every five time steps, at which point the pair list was also updated, and were kept unchanged between these updates. The cut-off radii were applied to the centres of geometry of the peptide charge groups and to the oxygen atoms of the methanol molecules.

The configuration of the molecular system in simulation MDT1 at time 200 ps was used to branch off two new MD simulations at higher temperatures, one at 350 K (MDT2) and one at 400 K (MDT3). Apart from the temperature, the parameter settings were the same as mentioned above. The total simulation time was, in each of the four MD simulations, 2200 ps. Every 0.5 ps configurations were saved for analysis.

In simulation MD DR we made use of a set of 42 NOE distances (Table 1) obtained by Seebach et al.[4] In order to make the system satisfy the NOE distance restraints, we used a time-averaged attractive distance-restraining interaction,[7, 11] with a force constant of $K_{dr} = 3000$ kJ mol^{-1} nm^{-2}, and a memory relaxation time of $\tau_{dr} = 50$ ps. When using this form of interaction, the (upper-bound) restraints are treated as quantities that have to be satisfied on average over time periods of given length (namely, 50 ps) during the course of the simulation.

Analysis: The NOE distances derived from experiment (Table 1) were compared to the distances derived from the simulations using an r^{-3} averaging. That is, the average effective violation of an NOE distance r_0 is calculated as $\langle r^{-3}\rangle^{-1/3} - r_0$, where r is the instantaneous distance at a given simulation time point. A set of 21 ^3J coupling constants derived from experiment (Table 2) were also compared to the corresponding ^3J coupling constants derived from the simulations. These were calculated using the Karplus relation [Eq. (1)],[8] where A, B and C were chosen to equal 6.4, −1.4, and 1.9 Hz, respectively, for the calculation of ^3J(HN,HC),[12] and to equal 9.5, −1.6 and 1.8 Hz, respectively, for the calculation of ^3J(HC,HC).[13]

$$^3J(\mathrm{H,H}) = A\cos^2\theta + B\cos\theta + C \quad (1)$$

Received: February 25, 1997 [F623]

[1] a) D. A. Plattner, A. Brunner, M. Dobler, H.-M. Müller, W. Petter, P. Zbinden, D. Seebach, *Helv. Chim. Acta* **1993**, *76*, 2004–2033; b) D. Seebach, T. Hoffmann, F. N. M. Kühnle, U. D. Lengweiler, *ibid.* **1994**, *77*, 2007–2034.

[2] H.-M. Müller, D. Seebach, *Angew. Chem.* **1993**, *105*, 483–509; *Angew. Chem. Int. Ed. Engl.* **1993**, *32*, 477–502; b) D. Seebach, A. Brunner, B. M. Bachmann, T. Hoffmann, F. N. M. Kühnle, U. D. Lengweiler, Ernst Schering Research Foundation, *Vol. 28*, **1995**, pp. 7–98.

[3] D. Seebach, M. Overhand, F. N. M. Kühnle, B. Martinoni, L. Oberer, U. Hommel, H. Widmer, *Helv. Chim. Acta* **1996**, *79*, 913–941.

[4] D. Seebach, P. E. Ciceri, M. Overhand, B. Jaun, D. Rigo, L. Oberer, U. Hommel, R. Amstutz, H. Widmer, *Helv. Chim. Acta* **1996**, *79*, 2043–2066.

[5] T. Hintermann, D. Seebach, *Synlett* **1997**, 437–438.

[6] D. H. Appella, L. A. Christianson, I. L. Karle, D. R. Powell, S. H. Gellman, *J. Am. Chem. Soc.* **1997**, *118*, 13071–13072.

[7] W. F. van Gunsteren, S. R. Billeter, A. A. Eising, P. H. Hünenberger, P. Krüger, A. E. Mark, W. R. P. Scott, I. G. Tironi, *Biomolecular simulation: The GROMOS96 manual and user guide*, vdf Hochschulverlag AG an der ETH Zürich and BIOMOS b.v., Zürich, Groningen, **1996**.

[8] M. Karplus, *J. Chem. Phys.* **1959**, *30*, 11–15.

[9] H. J. C. Berendsen, J. P. M. Postma, W. F. van Gunsteren, A. DiNola, J. R. Haak, *J. Chem. Phys.* **1984**, *81*, 3684–3690.

[10] J. P. Ryckaert, G. Ciccotti, H. J. C. Berendsen, *J. Comput. Phys.* **1977**, *23*, 327–341.

[11] a) A. E. Torda, R. M. Scheek, W. F. van Gunsteren, *Chem. Phys. Letters* **1989**, *157*, 289–294; b) A. E. Torda, R. M. Scheek, W. F. van Gunsteren, *J. Mol. Biol.* **1990**, *214*, 223–235; c) A. P. Nanzer, W. F. van Gunsteren, A. E. Torda, *J. Biomol. NMR* **1995**, *6*, 313–320; d) A. P. Nanzer, T. Huber, A. E. Torda, W. F. van Gunsteren, *J. Biomol. NMR* **1996**, *8*, 285–291; e) A. P. Nanzer, A. E. Torda, C. Bisang, C. Weber, J. A. Robinson, W. F. van Gunsteren, *J. Mol. Biol.* **1997**, *267*, 1012–1025.

[12] A. Pardi, M. Billeter, K. Wüthrich, *J. Mol. Biol.* **1984**, *180*, 741–751.

[13] A. de Marco, M. Llinas, K. Wüthrich, *Biopolymers* **1978**, *17*, 617–636.

  0947-6539/97/0309-1417 $ 17.50+.50/0